Original scientific paper

Informacije MIDEM
Journal of Microelectronics,
Electronic Components and Materials
Vol. 43, No. 1 (2013), 3 – 13

Optimization of grooved micromixer for microengineering technologies

Izidor Sabotin[1] Gianluca Tristo[2], Giuliano Bissacco[3] and Joško Valentinčič[1]

[1]Department of Manufacturing Technologies and Systems, University of Ljubljana, Slovenia
[2]Department of Industrial Engineering, University of Padua, Italy
[3]Department of Mechanical Engineering, Technical University of Denmark, Denmark

Abstract: Due to the absence of turbulent flow and the slow diffusion process, mixing of solutions at micro-scale is a difficult task. This paper describes the optimization route towards the efficient design of a bottom grooved micromixer. Based on thoroughly discussed mixing mechanisms, the optimization was performed using FEM numerical simulations and the starting geometry was a Staggered Herringbone Mixer (SHM) groove design. Optimization procedure consists of two sequences: (I) one SHM groove geometry is optimized based on the magnitude of transversal velocity at the end of the groove and (II) different configurations of six grooves are investigated taking into account capabilities and limitations of microengineering technologies (MET). Newly developed designs were benchmarked against the established SHM design and a better efficiency was achieved. Additionally, a good mixing efficiency was also achieved with a modified Slanted Groove Micromixer (SGM). A SGM prototype was machined by micro electrical discharge milling (EDM) technology. The simulation results were experimentally verified with flow visualization and a good agreement was observed. Due to simple 2.5D geometry and efficient mixing properties the proposed micromixer design is adequate to be used in the Lab-On-A-Chip (LOC) systems.

Keywords: micromixer, microstructures, micromachining, micro electrical discharge milling, microfluidics, design optimization, FEM simulations.

Optimizacija mikromešalnika z utori za izdelavo z mikroinženirskimi tehnologijami

Izvleček: Mešanje dveh tekočin v mikrokanalih je zaradi odsotnosti turbolentnih tokov in počasnega procesa difuzije oteženo. V prispevku je predstavljen pristop k optimizaciji geometrije mikromešalnika z utori. Za izhodiščno geometrijo je bil izbran kljukasti utor (SHM utor). Optimizacija je bila izvedena s pomočjo numeričnega modeliranja z metodo končnih elementov, upoštevajoč temeljne mehanizme delovanja mikromešalnika z utori. Optimizacija je bila izvedena v dveh korakih. Najprej je bila optimizirana geometrija enega SHM utora glede na povprečno velikost komponente hitrosti prečno na mikrokanal takoj za utorom. Nato je bil raziskan vpliv geometrije različnih konfiguracij šestih utorov, kjer so bile upoštevane zmogljivosti in omejitve mikroinženirskih izdelovalnih tehnologij. Nov dizajn izkazuje boljšo učinkovitost mešanja v primerjavi z uveljavljenim dizajnom. Dobro učinkovitost mešanja izkazuje tudi geometrija mikromešalnika s poševnimi utori (SGM geometrija). Za namen verifikacije simulacij je bil izdelan prototip SGM geometrije s tehnologijo mikro elektroerozijskega dolbenja. Rezultati simulacij so bili eksperimentalno verificirani z metodo vizualizacije toka fluida in opaženo je bilo dobro ujemanje. Zaradi preproste 2.5D geometrije mikrostruktur in učinkovitosti mešanja je predlagan dizajn mikromešalnika primeren za uporabo v sistemih laboratorija na čipu (LOC).

Ključne besede: mikromešalnik, mikrostrukture, mikroobdelava, mikro elektroerozijsko dolbenje, mikrofluidika, optimizacija dizajna, metoda končnih elementov, simulacije.

** Corresponding Author's e-mail: izidor.sabotin@fs.uni-lj.si*

1. Introduction

Miniaturization is a recent trend in analytical chemistry and life sciences as well as in non-silicon micromachining technologies [1,2]. In the past two decades, miniaturization of fluid handling and fluid analysis has emerged in the interdisciplinary field of microfluidics. A micromixer is a microstructured device and is an important component of a microfluidic system. Rapid mixing is essential in many of microfluidic systems used in biochemistry analysis, drug delivery, sequencing of synthesis of nucleic acids as well as in microreac-

tor systems [3-6]. Its function is to mix the reactants for initiation of the reaction process, and it is an indispensable component in lab-on-a-chip (LOC) platforms for complex chemical reactions. Micromixers can be integrated in a microfluidic system or work as stand-alone devices.

To mix solutions at the micro-scale is a difficult task. Under typical low Reynolds number operating conditions ($Re < 100$) the fluid flow is laminar. The absence of turbulent flow patterns and a slow diffusion process are the main challenges to overcome in order to achieve mixing. The ratio between the mass transport due to advection and that of diffusion is defined by Peclet number $Pe = vL/D$ where v denotes mean fluid velocity, L is a characteristic linear dimension of the channel geometry and D is a mass diffusion coefficient. In microchannels, the Peclet number is typically higher than 100, meaning a very slow diffusion process with respect to advection [7].

In contrast to active micromixers, where an additional source of energy has to be introduced into the microfluidic system (e.g. time-dependant electric or magnetic fields [8,9]), passive micromixers depend solely on pressure driven flow through the system relaying on enhancing mixing through lamination of the solute flow [10,11], injection of solute into a solvent flow [12], forming droplets of the mixed liquids [13] or inducing chaotic advection of the fluid flow by means of placing obstacles within the flow path [14,15], making a complex 2.5D channel geometry (e.g. modified Tesla structure [16]) or pattern the inner channel walls with oblique grooves [6,17-22]. Passive micromixers do not require external actuators. Therefore they are robust, stable in operation and easily integrated into more complex systems.

Bottom grooved micromixers attracted a lot of research interest due to the good mixing efficiency below $Re < 50$, small pressure drop, and established soft lithographic methods for its fabrication [6,17,19,20,22]. The most common geometries of grooved micromixers are the slanted groove micromixer (SGM) and the staggered herringbone micromixer (SHM), both embedded on the floor of the microchannel. The SGM grooves are inclined at an angle with respect to the axial direction, whereas the SHM grooves have the shape of a herringbone pattern (Fig. 1).

The oblique grooves serve to transport fluid from the apex of the groove structure to the downstream edges of the microchannel. Consequently, the fluid in the upper part of the channel starts to rotate in the opposite direction causing a helical flow pattern. The herringbone pattern of the SHM generates two counter-rotating helical flows and when alternating the asymmetry of the SHM grooves a chaotic flow profile is created. The circulating motion stretches and folds the fluids, which exponentially reduces the distance over which different molecules have to diffuse.

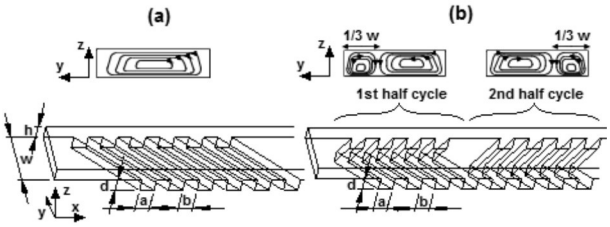

Figure 1: (a) Typical geometry of the slanted groove micromixer (SGM) and the schematic representation of streamlines in the channel cross-section. (b) Geometry of the staggered herringbone micromixer (SHM) and schematic representation of double helical motion caused by the groove geometry. One full cycle is composed of two half-cycles, one half-cycle has grooves oriented the same way.

To date, there have been a number of theoretical, experimental, and numerical studies aimed at the optimization of SGM and SHM geometry [6,17,23-30]. Different approaches were applied when optimizing the mixing efficiency of SGM and SHM geometries by means of numerical simulations. Hassel and Zimmerman [31] investigated convective motion through SHM geometries and used several flow based descriptors. They concluded that the efficiency of the groove in moving fluid cross channel could be reasonably described by the single groove case. Lynn and Dandy [24] defined a measure to quantify the magnitude of helical flow within the SGM by the ratio of non-axial to axial flow, normalized by the groove-ridge width and the channel width. They avoided the criteria of numerically simulated concentration fields due to possible numerical errors. Among the methods to quantify SHM and SGM mixing efficiency such as particle tracking [15,23,32,33], striation thickness [30], flow helicity [31], length of stretching [33,34], entropic measures [27], the relative variance of the concentration profile is most commonly used [14,16,25,26,34].

Experimentally, numerically simulated mixing behavior can be verified through the imaging of the concentration profile on the surface of the see-through micromixers by studying the change of color due to some chemical reaction of the fluid phases [6,15,18,19]. More detailed information at higher cost can be obtained by confocal microscopy [17,20,21]. Recently, Du et al. [6] verified the simulation results through fluorescent quenching experiments thus proving that numerically solved convection-diffusion equations give reliable information about mixing efficiency.

The SGM and SHM realizations reported in the literature have a lot of shallow grooves on the bottom of the mixing channel which suits the characteristics of soft lithographic manufacturing methods [6,17,19,20]. Thus, most of the optimization studies are limited to small deviations around the originally proposed geometry by Stroock et al. [17] which leads to local optimums within confined geometrical dimensions. The related papers provide a general trend about the geometry layout of microstructured grooves and its effects on mixing performance. However, the true optimum design has yet to be discovered for a specific application through numerical simulations [6].

For a successful micromixer design, it is important to consider the fabrication methods. In addition, microengineering technologies (MET) such as laser ablation, micromilling, micro EDM milling, etc. enable the fabrication of long life tools with high aspect ratio microstructures using, for example hardened steel or ceramics [1]. Thus, optimization of efficiency of every single groove is essential to minimize the costs of micromixer fabrication.

In this paper, a detailed insight into the design, optimization, analysis and performance of the grooved micromixer, suitable to be machined with micro EDM milling, is presented. The optimal geometry was benchmarked against established SHM design and the validity of simulations was checked with a flow pattern visualization of the optimized geometry. Special attention is given on the appropriateness of the design to be machined by non-silicon based micromanufacturing technologies and their limitations such as inability to produce sharp inner corners.

2. Materials and methods

2.1. Geometry of the micromixer

Original groove geometry of SHM, proposed by Stroock et al., was used as a starting geometry for mixer design optimization [17]. In Fig. 1(b), a typical structure of the SHM is shown which also denotes the variables used for groove optimization, namely *a* for the lateral groove width, *d* for groove depth and *b* for distance between two successive grooves. Primary flow flows along the *x*-axis, the *y*-axis is in the direction of the channel width and *z*-axis is in the direction of channel height.

The main channel width *w* and height *h* were fixed to $w = 200$ µm and $h = 50$ µm, since the selected channel size is commonly used channel cross section of commercially available microreactor systems [35,36].

The asymmetry of the SHM grooves was set to one third, meaning that the apex position of the groove is positioned at one third of the channel width, since that was found to be the optimal apex position in SHM design in the alternating half-cycle configuration [17,26]. The grooves are patterned at a 45° angle to the *x*-axis [17,26]. The total length of a simulated channel varied from 1.5 mm for simulations of one-groove geometry to 3.5 mm for six groove geometry. Preliminary simulations showed that only few optimized grooves were sufficient to complete the mixing. Thus the number of grooves for multiple groove configurations was fixed to six in order to show the efficiency of optimized one-groove geometry in comparison to established SHM geometry, and to maintain a design layout compatible with micro EDM milling technology. In line with the paradigm of design for manufacturing (DFM) the corners of groove geometries in multiple groove configurations were rounded to a minimum radius of $r_{groove} = 25$ µm which is readily achievable with micro EDM milling. Investigated groove parameters at different mixing regimes are gathered in Table 1.

2.2. Simulation tool

CFD modeling was performed using Comsol Multiphysics 4.1 which implements the finite element method (FEM) for numerical computation of physics governing equations. The numerical simulation was used to solve Navier-Stokes equations for incompressible fluid and convection-diffusion equations at steady state. The governing equations that describe the physical phenomena of mixing are as followed: Navier-Stokes (NS) equations,

$$\rho(\mathbf{v}\cdot\nabla)\mathbf{v} - \nabla\cdot\eta\left(\nabla\mathbf{v} + (\nabla\mathbf{v})^T\right) + \nabla p = 0,$$
$$\nabla\cdot\mathbf{v} = 0, \qquad (1)$$

Table 1: Presentation of parameters varied and configurations used: *a* – groove width, *d* – groove depth, *Re* – Reynolds number, *b* – ridge distance, r_{groove} – corner rounding, *D* – diffusion coefficient.

One-groove geometry			Six groove geometry, Re = 0.5, D = 10^{-9} m^2/s		
a [mm]	d [mm]	Re	b [mm]	r_{groove} [mm]	Configurations
0.05 – 0.30	0.03 – 0.20	0.5 - 20	0.05 – 0.35	0.025, 0.05*	SHM, SGM

* only in configuration of SGM_{rmax}

and convection-diffusion (CD) equations,

$$D\nabla^2 c - \mathbf{v}\cdot\nabla c = 0. \quad (2)$$

In equations 1 and 2 ρ denotes density [kg/m^3], $\boldsymbol{v}$ is the velocity vector [m/s], η denotes viscosity [Pa·s], p equals pressure [Pa], D denotes the diffusion coefficient [m^2/s] and c represents the concentration [mol/m^3].

Meshing of simulated geometries was implemented by the software applying free mesh elements that can easily adapt to the structure of the channel. The tetrahedral free meshing method with meshing parameters similar to that reported in literature was used [6,20]. Briefly, the computation of NS and CD equations was decoupled in order to reduce the computational power needed to run the simulation on a PC workstation (Intel i7 processor, 24 GB RAM). Maximum mesh element size for the main channel of the mixer used when solving NS equations was set to 15 µm, while the mesh in the grooves was set to 5 µm in order to reliably capture the fluid dynamics in the grooves. Maximum element size scaling factor was set to 0.2, element growth rate to 1.3, mesh curvature factor to 0.2 and the resolution of the narrow region to 1. Total number of mesh elements consisted of 2 to 6 x 10^5, depending on the simulated geometry. Mesh settings for solving CD equations were similar while reducing the maximum element size to 10 µm, resulting in 1 to 3 x 10^6 mesh elements. Finer adjustments of the mesh were performed in order to obtain the required convergence at a reasonable time scale while maintaining the required accuracy.

The fluid properties were set to the ones of water at 20˚C; density ρ = 998.2 kg/m^3 and viscosity η = 1.002 mPa·s. The diffusion coefficient of the solute was set to $D = 10^{-9}$ m^2/s since this is a typical value for most ions in aqueous solution. The inlet flows were set as inflows with average linear fluid velocity according to the *Re* regime investigated. The optimization of six groove geometries was conducted only for *Re* = 0.5, corresponding to v = 0.0063 m/s and a Peclet number of 630. The boundary condition for the outflow was set to 0 Pa (pressure, no viscous stress) and flow velocity at the walls to a no-slip condition (v = 0 m/s). Fluid concentration of one half of the channel was set to o 1 mol/m^3 (bright color) and the other half to 0 mol/m^3 (dark color) respectively. The post processing and visualizations of simulated results were obtained using the associated functions in Comsol and Matlab.

2.3. Optimization procedure

Measuring the quantity of the transversal flow is a logical predictor of the mixing efficiency [24,31]. Hassel and Zimmerman [31] also determined that peak values of non–axial velocities correspond to flow leaving the groove and that efficiency of the grooves in moving fluid cross channel could be reasonably described by the single groove case. These findings were utilized in presented optimization approach.

The optimization of the micromixer geometry was performed in two steps. In the first step, one-groove geometry was optimized based on the criterion of the average transversal velocity vector (Eq. 3). The average square root value of the velocity vector in directions perpendicular to primary flow (v_y, v_z) was calculated as

$$v_{AVGyz} = \frac{1}{N}\sum_i \sqrt{v_{y_i}^2 + v_{z_i}^2} \quad (3)$$

in the cut plane at the end of the single SHM groove (Fig. 2(a)), N denotes the number of points in the cut plane.

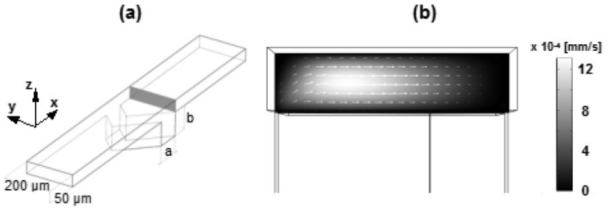

Figure 2: (a) Schematic presentation of single SHM groove geometry and the position of the cut plane where v_{AVGyz} is calculated. (b) Presentation of non-axial velocity field in *yz*-direction. Black and white color-coding denotes the amplitude of v_{AVGyz}.

In the second step an optimal 6 groove configuration, within the channel length of 3 mm, was determined by the criteria of relative variance of the concentration profile S at the distance x along the main channel length defined as,

$$S_x = \frac{\frac{s_x}{A_x}}{\frac{s_{inlet}}{A_{inlet}}}, \quad (4)$$

where s_x corresponds to variance of the concentration profile at particular cut plane,

$$s_x = \int_A (c_{xi} - c_\infty) dA, \quad (5)$$

where A denotes the *yz*-cut plane at coordinate x, c_{xi} denotes the concentration at a point on the cut plane and c_∞ denotes complete mixing, which is 0.5 mol/m^3 in our case. A value of S_x closer to 0 corresponds to better mixing performance.

2.4. Experimental setup

Based upon preceding geometry optimization a micromixer prototype was machined by micro EDM milling technology (Fig. 3(a)) in the tool steel (Fig. 11, configuration SGM_{rmax}—25). The lateral dimensions of the machined geometry were measured with optical microscope CETR, UMT Multi-Specimen Test System at a magnification of 550. Depth of micromixer structures was measured with a laboratory developed laser system with a resolution of 1 µm. The measured dimensions were:

- main channel width: $w = 203 \pm 4$ µm,
- main channel height: $h = 50 \pm 3$ µm,
- groove width: $a = 150 \pm 4$ µm,
- bottom groove depth: $d = 148 \pm 3$ µm.

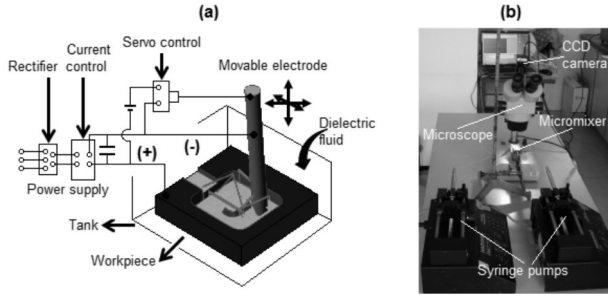

Figure 3: (a) Schematic presentation of micro EDM milling process. (b) Experimental setup.

Experimental setup is shown on Fig. 3(b). To seal the micromixer, a Plexiglas cover was bolted on the steel substrate which was polished to mirror finish before micro EDM milling. Plastic adapters were fitted for two inlets and one outlet. Two syringe pumps (PHD 4400, Harvard apparatus) were used to introduce two colored water phases into the micromixer. One phase was colored blue (Water blue, 5 g/l, dark color on grayscale figures) and the second one red (Congo red, 0.5 g/L, bright color on grayscale figures). These colored aqueous solutions provide a good contrast due to high solubility and large extinction coefficient of the dye. Due to the similar chemical structure of both solvents their diffusion coefficient is approximately the same and the reported value found in the literature corresponds to $D = 3.2 \cdot 10^{-10}$ m²/s [10].

A CCD camera (Image source DFK 22) was attached to the optical microscope with 100 times magnification and resolution of 4 µm per pixel. The inflow for each phase was set to 1.875 µl/min, which corresponds to an average fluid velocity of 6.3 mm/s.

Captured images were processed in MATLAB and RGB values of pixels at investigated cross sections were used to determine the phase borders. The results of simulation were verified via comparison of the course of the interface between both phases obtained by simulation and experiment.

3. Investigation of one-groove geometry

Investigation of one-groove SHM geometry was conducted under various *Re* regimes, namely from 0.5 to 20. The geometry parameters under investigation were lateral groove width *a* and groove depth *d*. Average transverse flow v_{AVGyz} induced by the groove was calculated at a cut plane at the end of the groove, and its dependence on groove geometry and flow regime is presented in Fig. 4. Values of v_{AVGyz} are normalized with the average fluid velocity along the *x*-axis, corresponding to each *Re* regime in order to make the comparison more transparent.

The amount of transversal fluid motion caused by the SHM groove, described by the parameter v_{AVGyz} is strongly dependent on the depth and width of the groove. For a fixed groove depth an optimal groove width exists; wider groove does not contribute to the increase of velocity v_{AVGyz} (Fig. 3). The same conclusion stands for groove depth. Beyond a certain groove depth the transversal motion of the fluid is not enhanced. This is due to the fact, that fluid near the bottom of deeper grooves has less impact on the flow profile (Fig. 5(a)). Therefore, for specific main channel geometry an optimal SHM groove geometry exists.

Optimal groove dimensions were considered at the intersection of the two asymptotes (Fig. 4). The first describes transversal motion of the fluid (v_{AVGyz}) at short groove widths ($a \rightarrow 0$) and the second corresponds to longer groove widths ($a \rightarrow \infty$); optimal groove depth at all simulated *Re* regimes corresponds to d_{opt} = 100 µm. Later observation is in line with findings that optimal groove depth is mainly determined by the channel aspect ratio [6,24]. By this characterization of optimal one-groove geometry, two important mixer efficiency conditions are satisfied: minimization of dead volume of the groove and minimization of volume to be removed by the micro EDM milling process in order to fabricate the geometry while maintaining the optimal mixing efficiency. The choice of d_{opt} = 100 µm is further clarified in Fig. 5(b), where at fixed $Re = 0.5$ and $a = 150$ µm the relative magnitude of v_{AVGyz} at $d = 100$ µm reaches 97.2% of the value of the deepest groove tested, $d = 200$ µm.

Fig. 4 shows the v_{AVGyz} dependence on the flow regime. Up to a *Re* number 10 the optimal groove dimensions are basically the same, i.e. groove width a_{opt} = 150 µm

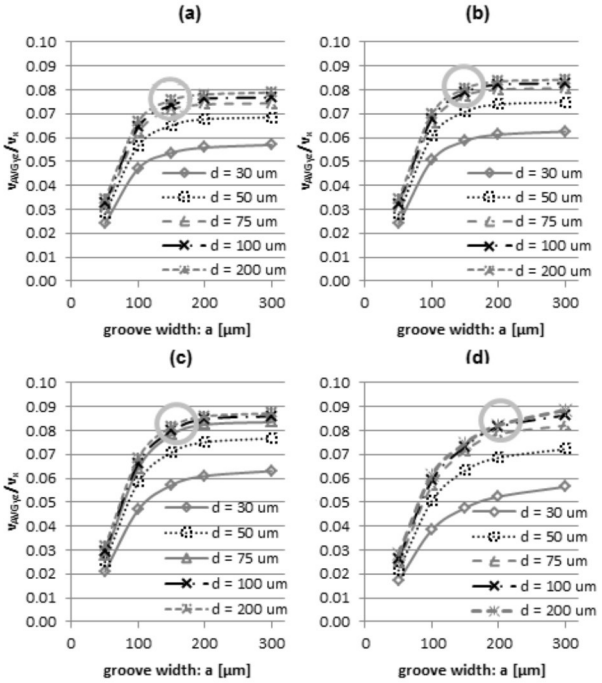

Figure 4: Dependence of relative magnitude of average transversal velocity (v_{AVGyz}/v_x) on SHM groove depth d and groove width a for (a) Re = 0.5, corresponding to average fluid velocity in x-direction of v_x = 6.3 mm/s, (b) Re = 5, v_x = 63 mm/s, (c) Re = 10, v_x = 126 mm/s and (d) Re = 20, v_x = 252 mm/s. Circles denote regions of optimal one-groove geometry dimensions.

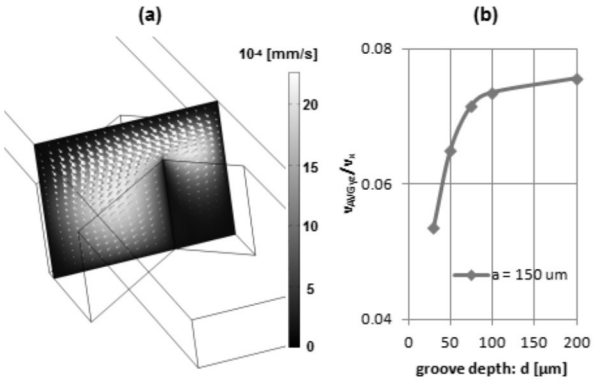

Figure 5: (a) Vector velocity field within the SHM groove, a = 150 μm, d = 100 μm. (b) Dependency of v_{AVGyz}/v_x on groove depth at fixed groove width a = 150 μm and Re = 0.5.

and groove depth d_{opt} = 100 μm. An evident shift towards a wider optimal groove dimension is seen at Re = 20, indicating a different flow behavior which can be explained as follows: greater the inertial forces, less fluid enters the groove. Increased inertia hampers the fluids ability to enter the groove and reduced viscous effects inhibit the ability of the entrained liquid in the groove to transfer momentum trough viscous stresses to the bulk flow. This conclusion is in line with the observations reported in the literature dealing with shallow grooves [20,31].

The efficiency of SHM is in strong connection with creating maximal cross channel fluid transfer. Yang et al. [26] concluded that the flow rate within the grooves of the SHM is substantiated as the most critical parameter of its efficiency which supports our choice of defining one-groove mixing efficiency by v_{AVGyz}. v_{AVGyz} is indirectly correlated with entrained fluid in the groove, namely, fluid cross channel transfer at the end of the groove is a consequence of momentum transfer of entrained fluid dragging the bulk flow due to viscous stresses.

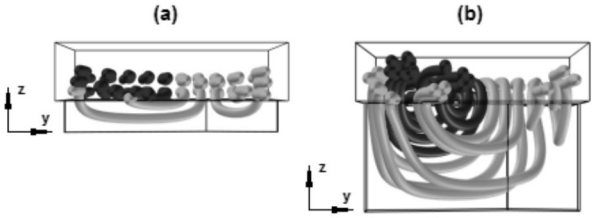

Figure 6: (a) Comparison of streamlines of one SHM groove at Re = 0.5, a = 50 μm, d = 30 μm and (b) a = 150 μm, d = 100 μm. Starting points of bottom row streamlines were set to 5 μm and upper row to 30 μm above channel floor. The amount of rotation of the streamlines after exiting the groove can be directly correlated to v_{AVGyz} parameter.

Another important mixing efficiency factor of one-groove geometry is evident from Fig. 6. As both fluid phases enter the groove the interface surface stretches and significantly increases the area over which diffusion takes place. Stretched interface surface is then folded in the bulk channel, further increasing the interface area by induced cross-channel convective motion resulting in greater mixing efficiency per groove.

4. Investigation of 6 groove configurations

4.1 Investigation of one full-cycle SHM configuration

Grooved micromixers are efficient only in sequences of multiple grooves. For established SHM configurations the grooves are organized into half-cycles, denoting a specific number of consequent grooves with the same apex orientation (Fig. 1(b)). In order to explore the cumulative effect, the influence of ridge distance b between two consecutive grooves on mixer performance, using one whole cycle SHM configuration was investigated. This configuration is denoted as SHM_6_3 meaning that six-grooves are organized in 3 grooves

per half-cycle (represented in Fig. 8, #3). The optimal geometry of a single groove determined in section 3 with a rounding of inner corners to r_{groove} = 25 µm was applied. The course of mixing along the length of the main channel (*x*-axis) for different ridge distances between consecutive grooves *b* is presented in Fig. 7.

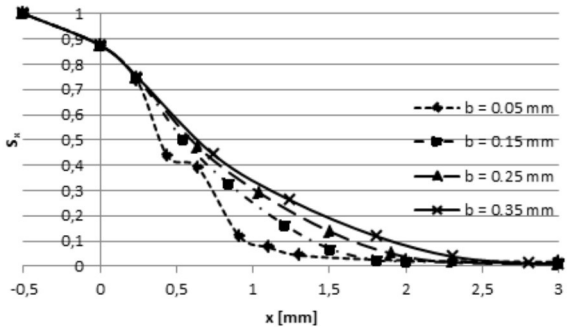

Figure 7: The course of mixing for SHM_6_3 configurations with different ridge distances *b*. First 0.5 mm is a grooveless section. Relative variance of the concentration profiles S_x was determined after every groove and at the exit of the channel (x = 3 mm).

The most efficient SHM_6_3 geometry is the one with the longest ridge distance tested b = 0.35 mm (Table 2). A plausible explanation of this result is as follows: if we presume that a single groove has a similar efficiency regardless of the ridge distance then in SHM_6_3_35 configuration the grooves are evenly distributed along the 3 mm main channel, enhancing the mixing process along the whole channel length, whereas in SHM_6_3_05 only 1.3 mm is effective. In the shortest configuration a reduction in the effectiveness at the cross-over region between half-cycles can be observed (Fig. 7, b = 0.05 mm, at x ≈ 0.5 mm).

In Table 2, an asymmetry around a mean concentration value of 0.5 can be noticed (c_{max}, c_{min}). This is due to the fact that a finite number of grooves are present in the simulated geometries, resulting in a skewed concentration distribution.

Efficiency of mixing can also be expressed with the minimum mixing length where 90% of the mixing is achieved. This value corresponds to the relative concentration variance value of S_x = 0.1 [25,26]. By this criterion the SHM_6_3_05 configuration is vastly superior to others, since 90% of mixing is achieved in the first 0.91 mm. On the other hand, from the production technology point of view, thin ridges could pose difficulties when manufacturing. From the results presented another important finding should be put forward: when dealing with a limited number of grooves the cumulative resonance effect, denoting an increased fluid entrainment due preceding groove(s) [23,24,26], does not outperform the configurations with longer ridge distances where cross channel convective motion decays, thus every groove fully exploits it's mixing potential. Due to the similar mixing performance the optimal ridge distance is between 0.25 and 0.35 mm for the given geometry.

It can also be inferred that in case of dealing with chemical solutions of slower diffusion constants and consequently higher Peclet numbers, the higher number of grooves is needed. If the optimization objective is mixing on the shortest distance possible, then ridge distance should be kept minimal, in this case 0.05 mm.

4.2 Investigation of six groove SHM and SGM geometry

The optimal number of grooves in a half cycle is not known in advance, thus all possible 6 groove SHM configurations were tested. In addition, the ridge distance b between the consecutive grooves was varied on the interval of 0.05 mm < b < 0.35 mm. Mixing efficiencies of simpler SGM groove configurations are also presented. Denotations of particular configurations are explained in Fig. 8. All the configuration tested exhibited the best mixing efficiency with the ridge distance b between 0.25 mm (Fig. 8, configurations #1, #2, #4, #6) and 0.35 mm (Fig. 8, configurations #3, #5, #7) implying that the optimal gap between consecutive grooves in order to fully exploit the potential of each single groove, should be in this range.

Among the tested configurations the most efficient one turned out to be SHM_6_2_25 (#1) based on both

Table 2: Presentation of mixing efficiency of the SHM_6_3 design with respect to ridge distance *b*. S_x – relative variance of concentration profile; c_{max} and c_{min} – maximum and minimum concentration value at x = 3 mm; *90% mix.* – length after 90% of mixing is achieved;

Ridge distance b [mm]	0.05	0.15	0.25	0.35
Configuration den.	SHM_6_3_05	SHM_6_3_15	SHM_6_3_25	SHM_6_3_35
S_x (x = 3 mm)	0.017	0.013	0.010	0.009
c_{max} (x = 3 mm)	0.615	0.610	0.614	0.633
c_{min} (x = 3 mm)	0.425	0.437	0.441	0.444
90% mix., (S_x = 0.1) [mm]	0.91	1.40	1.65	1.9

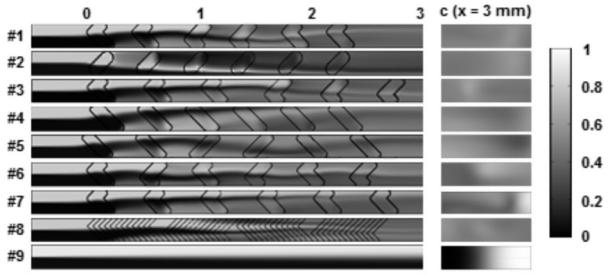

Figure 8: Best six groove SHM and SGM configurations at *Re* = 0.5 ordered from best to worst configuration. Configuration denotations are as followed: SHM_6_2_25 (#1), SGM_{rmax}_6_6_25 (#2), SHM_6_3_35 (#3), SGM_6_6_25 (#4), SGM_6_2_35 (#5), SHM_6_1_25 (#6) and SHM_6_6_35 (#7). Configuration #8 represents the benchmark geometry and #9 presents a grooveless channel. Explanation of specific configuration denotation: SHM or SGM_number of grooves_number of grooves in a half-cycle_ridge distance in tenths of millimeters. On the right part of the figure concentration profiles of the *yz*-cut plane at $x = 3$ mm are presented. The scale shows the color coding for concentrations.

criteria used, namely the lowest relative concentration variance and concentration profile at $x = 3$ mm (Figs. 9 and 10). The results show, that just 2 optimized grooves in a half-cycle by spatial transfer of the fluid efficiently stretch and fold both phases across the channel (Fig. 8, #1), which confirms the hypothesis of Lynn and Dandy [24] stating that only several grooves per half-cycle could be enough. In the first half-cycle the side with longer SHM groove arm is chiefly active. In the second half-cycle the longer arm switches position and exhibits strong mixing in that region. The last half-cycle further enhances mixing.

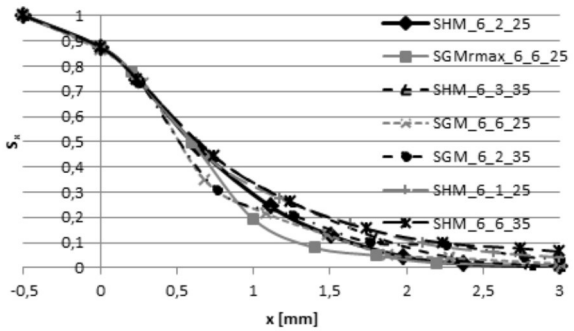

Figure 9: The course of mixing for the best 6 groove configurations optimized for ridge distance *b*. Relative concentration variance S_x is determined after every groove.

Surprisingly, due to the known fact of SHM geometry supremacy [6,17,24], SGM with the largest rounding radius, denoted as SGM_{rmax}_6_6_25 (#2), performed second best ($S_{3mm} = 0.008$) and significantly better than the #4 configuration with smaller corner radius. Due

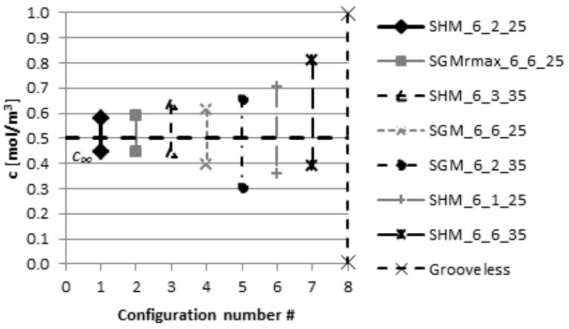

Figure 10: Minimum and maximum values of the concentration profile (c_{min} and c_{max}) for optimal 6 groove configurations at the outlet of the channel ($x = 3$ mm)

to largest corner rounding the configuration exhibited more complex rotation cycles which was also indicated by an increase of v_{AVGyz} by 45% in comparison to results obtained with sharp one-groove SGM geometry. It should be noted, that a significant part of increase of v_{AVGyz} is a consequence of a reference cut plane being closer due to groove rounding and thus direct comparison of the values would not be prudent. The poorly performing SGM_6_2_35 (#5) configuration, which can be viewed as an approximation of the #1 configuration without the shorter groove arms, highlights the important role of SHM's short arm.

Low mixing performance of SHM_6_1_25 (#6) configuration implies that one groove only does not transfer enough fluid across the main channel in order to promote stretching and folding of both fluid phases. The main reason for low efficiency is the effect of oppositely signed grooves, where the changing groove shape causes a reverse in directions of v_y and v_z, which results in dissipation of flow caused by the previous groove similarly observed by Hassell and Zimmerman [31].

The worst configuration of all tested was SHM_6_6_35 (#7). This is due to the obvious reason of the same orientation of grooves throughout the channel, thus the fluid in the shorter arm side remained very poorly mixed. On the other hand, good mixing is achieved in the longer arm section. This observation supports the hypothesis of Lynn and Dandy that the fluid flow within the long arm is the primary mechanism of mixing [24].

To show the adequacy of presented optimization procedure a benchmark simulation was performed applying established SHM design. Benchmark geometry was a slightly modified geometry proposed by Stroock et al. [17] with the main difference in the main channel cross-section which was fixed to ours ($h = 50$ µm, $w = 200$ µm). The benchmark micromixer, denoted as SHB, consisted of four half-cycles of 6 grooves with a groove depth of 35 µm, groove width of 50 µm and groove

ridge distance of 50 µm (Fig. 8 #8). Quantitative indexes show that SHM_6_2_25 design is more efficient compared to SHB design (Table 3). Thus, only six grooves of optimal dimensions compared to 24 grooves of established geometry are sufficient, making the final design compliant with the micro EDM milling technology.

Table 3: Comparison between benchmark SHB design and SHM_6_2_25 design. Values represent S_x – relative variance of concentration profile; c_{max} and c_{min} – maximum and minimum concentration value at x = 3 mm; *90% mix.* – length after 90% of mixing is achieved; p – pressure drop across the whole channel length.

Design	S_x (x = 3 mm)	c_{max} (x = 3 mm)	c_{min} (x = 3 mm)	90% mix., [mm]	p [Pa]
SHB	$6.95 \cdot 10^{-3}$	0.585	0.441	1.70	109.6
SHM_6_2_25	$4.87 \cdot 10^{-3}$	0.579	0.450	1.60	98.9

5. Experimental verification

In order to verify simulation results, a SGM_{rmax}–25 configuration was fabricated in tool steel by micro EDM milling starting with a 1 mm grooveless section before the first groove. Due to using the tool steel, verification methods which require see-through material could not be applied, thus actual mixing efficiency could not be determined. As the corresponding flow patterns are closely related to mixing efficiency [20], an indirect method via verification of the flow patterns was applied. A new simulation of mixing dynamics was performed using the diffusion constants of the experimentally used water coloring agents, namely $D = 3.2 \cdot 10^{-10}$ m^2/s. A good agreement of simulated and experimental flow patterns can be observed in Fig. 11.

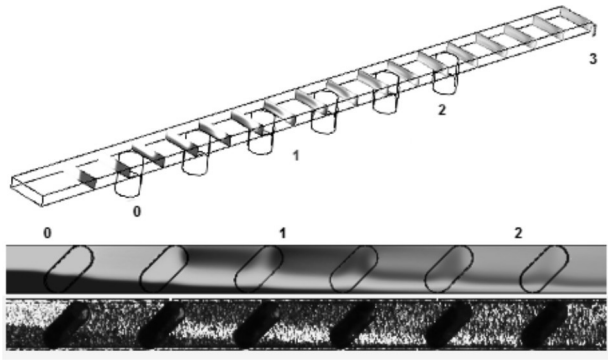

Figure 11: Experimental verification of the simulated flow pattern: on the upper part of the figure the dynamics of the water phases along the channel is presented. The middle picture shows the presence of both phases in the *xy*-plane at z = -25 µm. The bottom photograph of the experiment shows the course of the red phase (bright color) along the *x*-axis which closely resembles the simulated flow pattern.

In the upper part of Fig. 11 the principle of enhanced mixing by the SGM_{rmax} due to stretching and folding of the fluid phases, is presented. As both water phases start rotating in a clockwise direction, the interface layer dramatically increases. The brighter colored band can only be seen when the red phase occupies the whole vertical space from the top to the bottom of the channel, since this is also the direction of the channel observation through the microscope. For this reason a *xy*-plane at the height of z = -25 µm was selected as a cut plane to present results of the simulation and to compare the phase distribution along the *x*-axis with experimental results. The interface borders were detected by digital processing of the acquired pictures and obtained results are presented in Fig. 12. Excellent agreement of the course of the interface along the channel between both water phases is observed, thus it can be concluded that simulations reflect the real environment.

6. Conclusions

In the paper optimization procedure for grooved micromixer design suitable for microengineering technologies is presented. Principles behind grooved micromixer efficiency are thoroughly discussed and analyzed with FEM simulations. Optimization procedure can be easily applied in micromixer design stage.

Firstly, one groove geometry is optimized to maximize transversal fluid movement at the end of the groove. The simulation results revealed that for all Re regimes tested ($0.5 \leq Re \leq 20$), the optimal depth of the groove is 100 µm, but the groove should be wider in the case

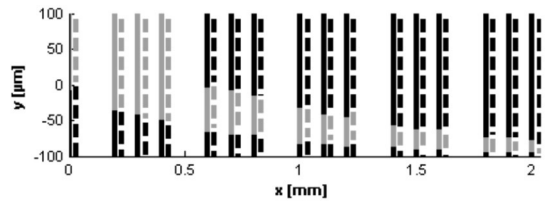

Figure 12: Detected interface border between two water phases with the bright color corresponding to the Congo red phase. A solid line is used for the simulation result at *xy*-plane of z = -25 µm and a dashed line for experimental results. The interface border was determined via computer image processing, in detail the amplitude of the R and B level of the RGB color scale were processed.

of higher Re regimes, thus optimal geometry of the groove is Re dependent.

In the second step, concentration parameters were used to quantify 6 groove configurations. Limitations and capabilities of micro EDM milling technology were considered. The results show that efficiency of mixing depends on configuration layout. The best configuration tested consisted of 2 grooves in a SHM half-cycle, which was benchmarked against an established SHM design with 2 full-cycles of 24 grooves and the new design performed better using only 6 grooves, making the design compliant with MET. The adaptation of the micromixer design to the manufacturing technology resulted in much simpler design with the same mixing capability as the original one.

Compared to the suggestions of the optimal grooved micromixer geometry found in literature our best groove design exhibits deeper and wider grooves. The mixing efficiency is further more enhanced through rounding of the groove corners.

A prototype of the optimized micromixer was produced by micro EDM milling. Experimental results were in good agreement with simulations. Furthermore, the micromixer was successfully applied in ionic liquid synthesis.

In the future work, optimized micromixer design will be used in a realization of a low cost microreactor system, made from polymers. Obtained microstructural geometries are suitable to be implemented with micro injection moulding technology.

Acknowledgments

This work is supported by Slovenian Research Agency (ARRS, Grant No. 1000-08-310-126 and Grant No. P2-0248). Authors wish to thank the members of Laboratory of Chemical, Biochemical and Environmental Engineering (Faculty of Chemistry and Chemical Tecnology, Uni. Lj.) for support on experimental verification and Laboratory of Biocybernetics (Faculty of Electrical Engineering, Uni. Lj.) for providing resources to run simulations.

References

1. Alting, L., Kimura, F., Hansen, H.N., Bissacco, G., (2003). Micro Engineering. CIRP Ann. Manuf. Technol. 52, 635–657.
2. Hessel, V., Lowe, H., Schonfeld, F., (2005). Micromixers - a review on passive and active mixing principles. Chem. Eng. Sci. 60, 2479–2501.
3. Pohar, A., Plazl, I., (2009). Process Intensification through Microreactor Application. Chem. Biochem. Eng. Q. 23, 537–544.
4. Cvjetko, M., Žnidaršič-Plazl, P., (2011). Ionic Liquids within Microfluidic Devices, in: Kokorin, A. (Ed.), Ionic Liquids: Theory, Properties, New Approaches. InTech., pp. 681-700.
5. Nguyen, N.-T., Wu, Z., (2005). Micromixers—a review. J. Micromech. Microeng. 15, R1–R16.
6. Du, Y., Zhang, Z., Yim, C., Lin, M., Cao, X., (2010). A simplified design of the staggered herringbone micromixer for practical applications. Biomicrofluidics 4, 024105.
7. Squires, T., Quake, S., (2005). Microfluidics: Fluid physics at the nanoliter scale. Rev. Mod. Phys. 77, 977–1026.
8. Bau, H., Zhong, J., Yi, M., (2001). A minute magneto hydro dynamic (MHD) mixer. Sens. Actuat. B-Chem. 79, 207–215.
9. Glasgow, I., Batton, J., Aubry, N., (2004). Electroosmotic mixing in microchannels. Lab Chip 4, 558–562.
10. Hessel, V., Hardt, S., Lowe, H., Schonfeld, F., (2003). Laminar mixing in different interdigital micromixers: I. Experimental characterization. Aiche J. 49, 566–577.
11. Schönfeld, F., Hessel, V., Hofmann, C., (2004). An optimised split-and-recombine micro-mixer with uniform "chaotic" mixing. Lab Chip 4, 65–69.
12. Voldman, J., Gray, M., Schmidt, M., (2000). An integrated liquid mixer/valve. J. Microelectromech. S. 9, 295–302.
13. Paik, P., Pamula, V.K., Fair, R.B., (2003). Rapid droplet mixers for digital microfluidic systems. Lab Chip 3, 253.
14. Wang, H., Iovenitti, P., Harvey, E., Masood, S., (2002). Optimizing layout of obstacles for enhanced mixing in microchannels. Smart Mater. Struct. 11, 662–667.
15. Bhagat, A.A.S., Papautsky, I., (2008). Enhancing particle dispersion in a passive planar micromixer using rectangular obstacles. J. Micromech. Microeng. 18, 85005.
16. Hossain, S., Ansari, M., Husain, A., Kim, K., (2010). Analysis and optimization of a micromixer with a modified Tesla structure. Chem. Eng. J. 158, 305–314.
17. Stroock, A., Dertinger, S., Ajdari, A., Mezic, I., Stone, H., Whitesides, G., (2002). Chaotic mixer for microchannels. Science 25, 647–651.
18. Johnson, T., Ross, D., Locascio, L., (2002). Rapid microfluidic mixing. Anal. Chem. 74, 45–51.
19. Kim, D., Lee, S., Kwon, T., Lee, S., (2004). A barrier embedded chaotic micromixer. J. Micromech. Microeng. 14, 798–805.

20. Williams, M., Longmuir, K., Yager, P., 2008. A practical guide to the staggered herringbone mixer. Lab Chip 8, 1121–1129.
21. Tofteberg, T., Skolimowski, M., Andreassen, E., Geschke, O., 2010. A novel passive micromixer: lamination in a planar channel system. Microfluid. Nanofluid. 8, 209–215.
22. Sato, Yagyu, D., Ito, S., Shoji, S., 2006. Improved inclined multi-lithography using water as exposure medium and its 3D mixing microchannel application. Sensor. Actuat. A-Phys. 128, 183–190.
23. Wang, H., Iovenitti, P., Harvey, E., Masood, S., 2003. Numerical investigation of mixing in microchannels with patterned grooves. J. Micromech. Microeng. 13, 801–808.
24. Lynn, N., Dandy, D., 2007. Geometrical optimization of helical flow in grooved micromixers. Lab Chip 7, 580–587.
25. Ansari, M.A., Kim, K.-Y., 2007. Application of the Radial Basis Neural Network to Optimization of a Micromixer. Chem. Eng. Technol. 30, 962–966.
26. Yang, J., Huang, K., Lin, Y., 2005. Geometric effects on fluid mixing in passive grooved micromixers. Lab Chip 5, 1140–1147.
27. Fodor, P.S., Itomlenskis, M., Kaufman, M., 2009. Assessment of mixing in passive microchannels with fractal surface patterning. Eur. Phys. J-Appl. Phys. 47, 8.
28. Zhang, Z., Yim, C., Lin, M., Cao, X., 2008. Quantitative characterization of micromixing simulation. Biomicrofluidics 2, 014101.
29. Du, Y., Zhang, Z., Yim, C., Lin, M., Cao, X. (2010) Evaluation of Floor-grooved Micromixers using Concentration-channel Length Profiles. Micromachines 1(1), 19-33.
30. Aubin, J., Fletcher, D., Xuereb, C., (2005). Design of micromixers using CFD modelling. Chem. Eng. Sci. 61, 2503–2516.
31. Hassell, D., Zimmerman, W., (2006). Investigation of the convective motion through a staggered herringbone micromixer at low Reynolds number flow. Chem. Eng. Sci. 61, 2977–2985.
32. Aubin, J., Fletcher, D., Bertrand, J., Xuereb, C., (2003). Characterization of the mixing quality in micromixers. Chem. Eng. Technol. 26, 1262–1270.
33. Kee, S., Gavriilidis, A., (2008). Design and characterisation of the staggered herringbone mixer. Chem. Eng. J. 142, 109–121.
34. Song, H., Yin, X., Bennett, D., (2008). Optimization analysis of the staggered herringbone micromixer based on the slip-driven method. Chem. Eng. Res. Des. 86, 883–891.
35. Žnidaršič-Plazl, P., Plazl, I., (2009). Modelling and experimental studies on lipase-catalyzed isoamyl acetate synthesis in a microreactor. Process Biochem. 44, 1115–1121.
36. Novak, U., Pohar, A., Plazl, I., Žnidaršič-Plazl, (2012) . Ionic liquid-based aqueous two-phase extraction within a microchannel system. P. Separ. Purif. Technol., doi:10.1016/j.seppur.2012.01.033.

Arrived: 16. 08. 2012
Accepted: 20. 01. 2013